Biochemistry & Physiology: Open Access

Kumar et al., Biochem Physiol 2016, 5:1
DOI: 10.4172/2168-9652.1000194

Research Article Open Access

Synthesis of Dox Drug Conjugation and Citric Acid Stabilized Superparamagnetic Iron-Oxide Nanoparticles for Drug Delivery

Pramod Kumar*, Shrish Agnihotri and Indrajit Roy

Department of Chemistry, University of Delhi, Delhi-110007, India

Abstract

In this manuscript, we report a novel, low cost and easy synthesis, iron-oxide nanoparticles were synthesized via room-temperature reduction of a mixture of ferric and ferrous salts, containing citric acid as capping agent. Next, anticancer drug doxorubicin (Dox) was used to form electrostatic conjugation with these nanoparticles. The resulting drug-nanoconjugates were characterized for their size, composition, functionality, crystallinity, along with their magnetic and optical behavior. Following that, they were treated with cultured lung carcinoma cell lines (A 549) to probe their non-toxicity and biocompatibility. Concurrently, their uptake in cells in culture was studied by optical bioimaging. *In vitro* studies have shown that these nanoparticles are nontoxic (using MTT assay) to cells in culture.

Keywords: Fe_3O_4; DOX; Dox-CA-SPION; VSM

Introduction

One of the major challenges in Nanomedicine is targeted delivery of drugs to target sites of interest that is to increase the concentration of drug on desired sites relative to others and to enhance the interaction of drug to diseased tissues rather than healthy tissues. Drugs in their free form, once administered systemically in the body, usually diffuse to different parts of the body. As a result, not only very little drug reaches the intended site of action (e.g. Diseased site), but also causes unwanted side effects in non-target organs. Therefore, it is critically important to devise ways to concentrate the drug at the diseased site for improved therapeutic outcome. Nanoparticle-based drug delivery can reduce this problem partially by using receptor-mediated drug delivery, whereby biorecognition agents (ligands) attached with drug-nanoparticle conjugates can guide the drugs to targeted sites [1-4]. However, the preparation of such targeted nanoformulations in optimal proportions is difficult, and often results in their uncontrolled size increase. Furthermore, these targeted nanoformulations may become immunogenic as most biorecognition ligands are protein/peptide based. An alternative way of nanoparticle-mediated targeted drug delivery involves transport the drug-nanoparticle conjugates to target sites using external stimulus, such as light and magnetic field [5-8]. Magnetic field assisted drug delivery is highly promising as it involves the use of non-ionizing radiation with no restriction on their penetration depth across biological tissues. Although this mode of drug delivery was restricted to already-identified and localized diseased sites, it nevertheless offers great promise in side-effect free treatment of diagnosed solid tumors and other malignancies.

Iron-oxide nanoparticles are extremely promising for medical applications owing to their ultra-small size, superparamagnetic properties, ease of synthesis, and biocompatibility [9-12]. Their most popular application is contrast enhancement in magnetic resonance imaging (MRI) [13-16]. Moreover, their ability to readily respond to external magnetic field has led to several promising applications, such as magnetic field-directed cell separation, triggering of local hyperthermia for localized anticancer activity, and magnetically-guided drug delivery [17,18]. Magnetic field assisted delivery of active molecules by iron-oxide nanoparticles can lead to several medical benefits, which include targeted delivery of chemotherapeutic agents for combination of MRI diagnostics and chemotherapy (theranostics), combination with optical agents for combined MR and optical imaging, etc. [19-22].

In this work, iron-oxide nanoparticles were synthesized via room-temperature reduction of a mixture of ferric and ferrous salts, containing citric acid as capping agent. Further, anticancer drug doxorubicin (Dox) was used to form conjugates with these nanoparticles. The resulting drug-nanoconjugates were characterized for their size, composition, functionality, crystallinity, along with their magnetic and optical behavior. Following that, they were treated with cultured lung carcinoma cell lines (A-549) *in vitro*, as well as whole blood, to probe their non-toxicity and biocompatibility. Concurrently, their uptake in cells in culture was studied, with and without magnetic guidance. Finally, the effect of drug-conjugated nanoparticles to cause drug-induced cytotoxicity in cells *in vitro* was investigated, with and without magnetic guidance.

Experimental Section

Materials

Ferric chloride ($FeCl_3.6H_2O$), ferrous sulphate ($FeSO_4.6H_2O$), ammonia solution (25%), was purchased from Merck. Doxorubicin hydrochloride (Dox), 2,9-dimethyl (1,10-phenanthroline), 3-(4,5-dimethylthiazol-2-yl), 5-diphenyltetrazolium bromide (MTT reagent), fetal bovine serum (FBS), phosphate buffer saline (PBS), Dulbecco's modified eagle's medium (DMEM), penicillin/streptomycin, and amphotericin-B were purchased from Sigma-Aldrich. Citric acid monohydrate (CA) was purchased from Spectrochem Pvt. Ltd. (Mumbai, India). Lung carcinoma cell lines (A-549) were purchased from ATCC, VA, and cultured according to instructions supplied by the vendor. Unless otherwise mentioned, cell culture products were obtained from Thermo Fisher scientific. All chemicals were used without any further purification.

Synthesis of citric acid stabilized superparamagnetic iron oxide nanoparticles (CA-SPION)

Synthesis of citric acid stabilized superparamagnetic iron-oxide

***Corresponding author:** Pramod Kumar, Department of Chemistry, University of Delhi, Delhi-110007, India, Tel: +91-9711065966; E-mail: pramodgang03@gmail.com

Received December 10, 2015; **Accepted** January 06, 2016; **Published** January 13, 2016

Citation: Kumar P, Agnihotri S, Roy I (2016) Synthesis of Dox Drug Conjugation and Citric Acid Stabilized Superparamagnetic Iron-Oxide Nanoparticles for Drug Delivery. Biochem Physiol 5: 194. doi: 10.4172/2168-9652.1000194

nanoparticles (CA-SPIONs) at room temperature has been carried out using the chemical precipitation method [23,24]. The aqueous solution of 2 mmol of $FeCl_3.6H_2O$, 1 mmol of $FeSO_4.6H_2O$, and 1 mL of HCl solution (50 µL 12 N HCl diluted to 1 mL by DDW) was mixed with 40 mL N_2 gas-purged double distilled water (DDW). Synthesis of the nanoparticles was accomplished by the addition of iron salt solution to 5 mL aqueous ammonia solution (25%) drop-wise with vigorous stirring for 30 seconds, resulting in dark suspension of SPION. After that the stabilizer solution, i.e., 1 mL aqueous (0.5 mg/mL) citric acid, was added and further stirring carried out for 30 minutes at room temperature. The resulting CA-SPION mixture was purified via centrifugation (10,000 rpm, 10 minutes) and washed with 2-3 times with ethanol and finally resuspended in water just by sonication for 10 minutes at bath sonicator.

Formation of electrostatic conjugates of doxorubicin with CA-SPION (Dox-CA-SPION)

The Dox-CA-SPION conjugates were formed by reaction of CA-SPION with excess Dox in aqueous phase. The free carboxylic acid groups on the surface of CA-SPION electrostatically-reacted with the amino groups present in Dox. Here, 50 µL aqueous dispersion of CA-SPION (2 mg/mL) was added to a 1 mL of Dox solution (10 mg/mL in DMSO), and mixed with shaking at room temperature for 2 minutes [25]. After formation of the drug-nanoparticle conjugates, they were separated from the free drugs via magnetic separation and washing in the aqueous medium.

Characterization Studies

The magnetic properties of the dried nanoparticles were probed using vibrating sample magnetometer (VSM), using a Model 3463-60 Electromagnet Amplifier (CREST Performance CPX 900 power amplifier Instrument). The sizes of the CA-SPIONs, with and without Dox conjugation, were determined using transmission electron microscopy (TEM). For TEM, the aqueous dispersions were sonicated and dropped-coated and dried onto formvar coated 200 mesh, copper grids (Ted Pella, USA), followed by imaging using a TECNAI G2-30 U TWIN TEM instrument (FEI, Eindhoven, The Netherlands) with an acceleration voltage of 300 KV. The same instrument was used for probing the elemental composition (using energy dispersive spectroscopy, or EDX) and crystalline diffraction pattern (using selected area electron diffraction, or SAED) of the nanoparticles. The Size of the nanoparticles was further analyzed by dynamic light scattering (DLS) measurements, using a NANO-ZS series MALVERN ZETASIZER instrument. Helium-Ne laser (wavelength 633 nm, power 4 mW) was used as the light source. The same instrument was used to measure the surface charge (zeta potential) of the nanoparticles. High resolution powder x-ray diffraction (XRD) was used to analyze the phase composition of the nanoparticles, using a Brukar D8 Discover x-ray spectrometer, over the 2θ range from 20°–65° at a rate of 2.58/min, using Cu-Kα radiation (λ=1.54060 Å). The UV-visible absorption and fluorescence emission measurements of the various aqueous nanoparticulate samples, both with and without conjugated Dox, were recorded using a Shimadzu UV-1601 spectrophotometer (Shimadzu, Kyoto, Japan) and a Cary Eclipse fluorescence spectrometer (Varian, Palo Alto, CA), respectively. FTIR spectra (resolution: 4 cm^{-1}) were acquired using a Perkin Elimer RX1 spectrometer, where 2 mg of dried and powdered nanoparticles were mixed with KBr and pressed into a pellet for analysis. The spectrum was taken from 4000 to 400 cm^{-1}. NMR Spectra were taken using a 400-MHz spectrometer (JNM-ECX-400P; JEOL, Tokyo, Japan).

Determination of drug loading efficiency

For determining the drug loading efficiency, the Dox-CA-SPION conjugates were first separated from free Dox in solution via magnetic separation. The fluorescence spectra of the supernatant obtained after magnetic separation of free Dox from Dox-CA-SPION) were then recorded using Cary Eclipse fluorescence spectrophotometer. The fluorescence spectra of 1 mL of pure Dox solution (10 mg/mL) were also taken. For comparison the fluorescence spectrum of initial amount of pure Dox aqueous solution (50 µL of 1.72 Mm Dox conc.=85 µM). The fluorescence intensities of supernatants (washed drug molecules were also taken into consideration for calculations) against pure Dox solution were used to determine the loading efficiency.

The loading efficiency (w/w %) was calculated using the following relation:

Drug loading (%) = [(Weight of drug in NPs) / (Weight of drug in NPs)] × 100

Drug entrapment efficiency (%) = [(Weight of drug in NPs) / (Weight of drug in NPs)] × 100

Drug-release studies

We have investigated the time-dependent release behavior of Dox from Dox-CA-SPION by dialyzing them in a solution containing PBS for 70 hours. As owing to the low cutoff (12-14 KDa) pore size of the dialysis membrane only free Dox molecules can come out of the membrane, we have estimated the amount of released Dox by measuring the Dox concentration (via fluorescence spectrometry) in the bulk solution as a function of dialysis time.

In vitro studies

We first probed the potential toxicity of these nanoparticles (drug-free) in the blood, using hemolysis assay. After that, we carried out studies probing the interaction of these nanoparticles, with and without linking drug, using A-549 lung cancer cells *in vitro*. These cells were maintained in DMEM medium with 10% FBS and 1% antibiotics (Penicillin and Streptomycin), and cultured according to manufacturer's instructions.

Analysis of potential *in-vitro* cytotoxicity of SPION and CA-SPION

We then investigated the potential non-specific cytotoxicity of non-drug conjugated SPIONs and CA-SPIONs in A-549 cells using cell viability (MTS) assay. One day prior to treatment, the cells were trypsinized and resuspended in fresh media. Then, about 25,000 cells/0.5 mL media were added to each well of a sterilized 24-well plate, and transferred back to the incubator for attachment and overnight growth. Next day, to the cells at a confluence of 30-40%, three different dosages of SPIONs and CA-SPIONs were added, mixed by swirling, and transferred back to the incubator. Control cells received PBS treatment only. After 48 hours of incubation, the plate containing the cells was taken out, the cells in each well were washed 3 times with sterile PBS, and treated with 100 µL of MTS reagent [3-(4,5-dimethylthiazol-2-yl)-2,5-diphenyltetrazolium bromide, (5 mg/mL in PBS)] for 2 hours. The resulting blue-colored formazan crystals were dissolved in DMSO, and their optical densities were recorded at 570 nm using UV–visible spectrophotometry. The optical density of each solution reflected the viability of the cells in each well. The percentage viability of the treated cells was calculated after comparing their optical density with that of PBS treated cells (positive control), the latter being arbitrarily assigned 100% viability [26,27].

Monitoring of cellular uptake of drug-doped (Dox-CA-SPION) nanoparticles *in vitro* via fluorescence microscopy

After probing the potential toxicity of non-drug linked nanoparticles in the blood and A-549 cells, we began our analysis of interaction of drug-linked nanoparticles (Dox-CA-SPIONs) with A-549 cells *in vitro*. Here, first we monitored the cellular uptake of the drug-linked nanoparticles. One day prior to treatment, the A-549 lung cancer cells were seeded in sterilized 6-well plates (2,00,000 cells/ 2 mL media in each well) and kept in the incubator. Next day, to the cells at a confluence of 60–70%, 2 mg/ml of Dox-CA-SPION sample were added, mixed by swirling, and kept in the incubator for 2 hours. After incubation, the plate was taken out and the cells in each well washed twice with sterile PBS, and fixed by a mixture of methanol and glycerol. The fixed cells were visualized under a fluorescent Nikon TS-100 inverted microscope, and photographed using a Nikon DIGITAL SIGHT DS-Fi1 Camera (Nikon, Japan). The fluorescence of Dox observed from the cells qualitatively correlated with the nanoparticle uptake.

Results and Discussion

Figure 1A shows the magnetization curves of the superparamagnetic iron-oxide nanoparticles, without (SPION) and with (CA-SPION) coated with citric acid. These curves were recorded at room temperature using vibrating sample magnetometer (VSM). Under a large external field, the magnetization of the particles aligns with the field direction and reaches its saturation value for both these nanoparticles. This pattern is indicative of superparamagnetic nanoparticles [26]. The saturation magnetization (Ms) values of SPION and CA-SPION were 68.0 and 58.0 emu/g, respectively. This result shows that citric acid coating did not significantly alter the magnetic behavior of SPION. Figure 1B shows the colloidal stability of aqueous dispersed CA-SPION, which does not have a tendency to precipitate and settle down. However, these nanoparticles can be separated from the bulk solution upon exposure to magnetic fields. This is shown in Figure 1C, where CA-SPION nanoparticles separate from solution and migrate towards the glass surface in contact with an external bar magnet. This data shows that these nanoparticles can be controlled using external magnetic force.

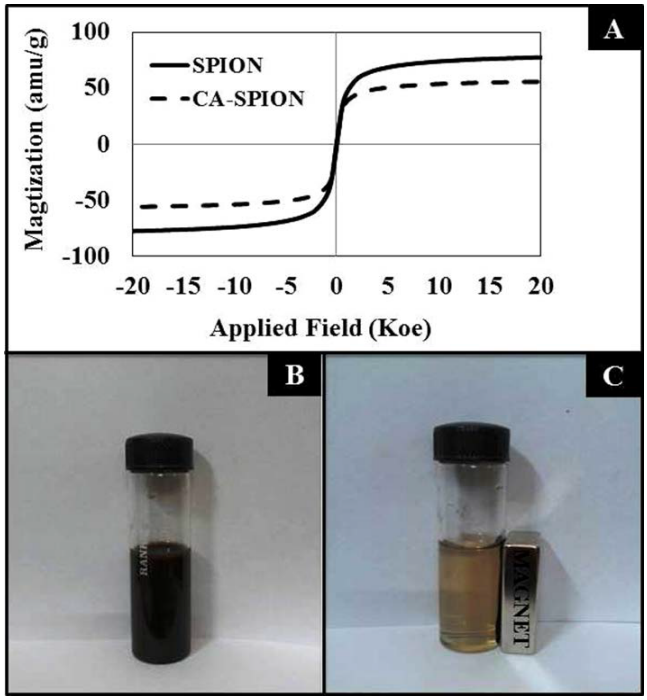

Figure 1: (A) Magnetization curves of superparamagnetic iron-oxide nanoparticles (SPION) and citric acid stabilized SPION (CA-SPION). (B, C) Photographs showing (B) dispersed CA-SPION in water in the absence of magnetic force, and (C) separated CA-SPION migrating to one side of the glass surface under magnetic force.

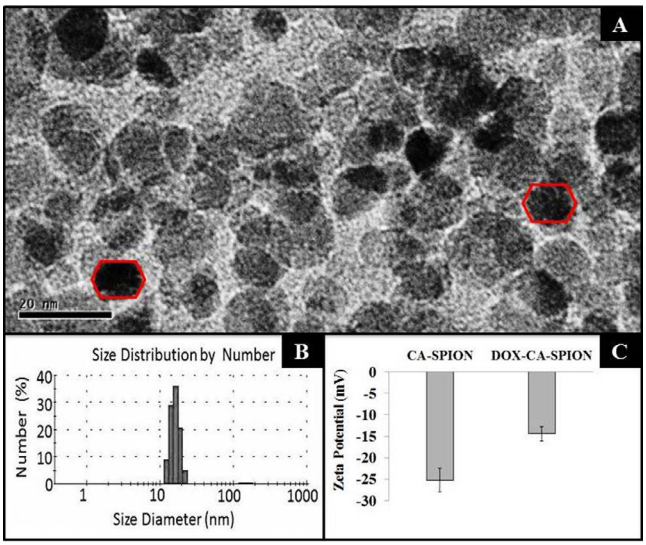

Figure 2: (A) TEM pictures of CA-SPION, showing their uniformity of size (Scale bar=20 nm). (B) DLS data showing hydrodynamic diameters (number average size distribution) of aqueous dispersions of CA-SPION. (C) Surface charge (zeta potential) values of CA-SPION and Dox-CA-SPION.

The TEM images of the synthesized CA-SPION are shown in Figure 2A, showing them to be irregular in size, with an average diameter of about 12 nm. Their size has been further determined by dynamic light scattering (DLS), which measures the hydrodynamic diameter of the nanoparticles. Figure 2B shows the mean hydrodynamic diameter of CA-SPION to be 25 nm. The DLS data are in good accordance with the TEM results, as the DLS determines the hydrodynamic diameter (nanoparticle diameter+hydration layer) of nanoparticles, which is always higher than the actual nanoparticle diameter given by TEM analysis. The surface charge (zeta potential) of CA-SPION, with and without Dox conjugation, is shown in Figure 2C. The zeta potential values of CA-SPION and Dox-CA-SPION are -26.6 mV and -14.6 mV, respectively. This can be explained by the fact that the negative surface charge of CA-SPION, owing to anionic carboxylate groups on their surface, are partially reduced in Dox-CA-SPION by the cationic Dox molecules electrostatically attached to their surface.

Figure 3A represents the XRD spectrum of the CA-SPION, showing diffraction peaks of (200), (311), (400), (422), (440) and (500), which match the characteristic peaks of the inverse spinel structure of Fe_3O_4 (Magnetite, JCPDS card no. 77-1545). The diffraction peaks delineate face-centered lattice (fcc) and cubic unit cells of nanoparticles. The clarity of XRD peaks indicated the crystalline nature of the nanostructures. Figure 3B confirms the crystalline pattern, as observed from the clearly visible diffraction rings in the SAED data. The elemental composition of these nanoparticles is provided in their EDX spectra (Figure 3C), showing the presence of iron and oxygen. The presence of copper and carbon is due to the composition of the grid (carbon coated copper grids) on which the nanoparticles were loaded.

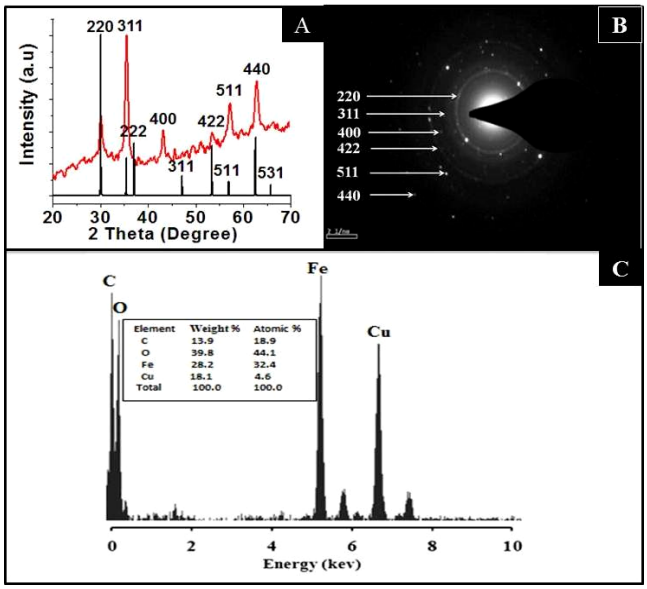

Figure 3: (A) Power X-ray diffraction (XRD) spectrum of CA-SPION (red), overlaid with that of the inverse spinel structure of Fe_3O_4 (black lines). (B) SAED pattern of CA-SPION, with clear diffraction rings, and (C) EDX spectra of CA-SPION.

The surface modification of SPION via coating with CA is shown by the FTIR analysis of SPION, CA and CA-SPION (Figure S1, Supplementary Data). The spectrum of SPION shows the presence of a characteristic peak for Fe-O-Fe as a strong band at 590–605 cm^{-1}. A prominent and broad peak at 3450-3515 cm^{-1} clearly revealed the presence of numerous surface hydroxyl groups on the surface of SPIONs. The FTIR spectrum of CA shows absorbance peaks at 1668 cm^{-1} (C=O), 2918 cm^{-1} (CH_2 stretching) and 2918 cm^{-1} (C–H symmetric stretch), along with one broad peak around 3450 cm^{-1} (OH-stretching vibration). In the spectrum of CA-SPION, all the peaks match those found in SPION and CA, with the exception of carbonyl (C=O) peak of CA, which has slightly shifted as a result of CA attachment to SPION surface [28,29].

The optical properties of the Dox-loaded nanoparticles (Dox-CA-SPION) have been studied by UV-visible and fluorescence spectroscopies. For comparison, the spectrum of free Dox and CA-SPION are also recorded. Figure 4A presents the absorption spectrum, showing that the absorption peak of free Dox (at 490 nm) is reduced and slightly blue shifted upon conjugation with CA-SPION. The same pattern is reflected in the fluorescence spectrum of the above samples, following excitation at 490 nm (Figure 4B). The typical fluorescence spectra of Dox are shown, with peaks at 560 and 590 nm, with most intense peak at 590 nm. The fluorescence intensity of free Dox is significantly reduced upon conjugation with CA-SPION. This can be attributed to the fact that iron-oxide is known to quench the fluorescence of fluorophores. Nevertheless, the Dox-CA-SPION sample still has enough optical signal that can be used in bioimaging applications.

We next investigated whether the fluorescent drug Dox can be released from the Dox-CA-SPION nanobioconjugates. Figure 5 presents the release kinetic data of the fluorescent drug Dox from the Dox-CA-SPION, at pH 5 and 7 (both at 37°C). It can be seen that the drug is released from the nanoparticles in a sustained manner, with about 70% and 90% release in 70 hours. This data demonstrates that these nanoparticles can be used as a slow release drug delivery vehicle.

After synthesis and characterization, we investigated the interaction of these nanoparticles with cells *in vitro*. First, we ascertained the potential non-specific cytotoxicity of CA-SPION, along with drug induced toxicity of Dox-CA-SPION. For that, we have treated living cells with these nanoparticles and analyzed the cell viability. It can be seen from Figure 6A that after 48 hours of treatment with three different dosages (H: High dose; M: Medium dose; and L: Low dose) of SPION, CA and SPION-CA, the cells remained more than 95% viable, even at a dosage as high as 400 µg/mL. This data demonstrates that the SPION, whether in free form or citric acid coated, exert negligible toxic effects on the cells. However, upon treatment with drug-conjugated nanoparticles (Dox-CA-SPION), significant cytotoxicity has been observed (about 45% cell viability), although it is lower than the cytotoxicity of free Dox (about 25% cell viability). This means that the drug conjugated nanoparticles can function in drug delivery. It is worth noting that free Dox is cardiotoxic, and therefore it can be applied in *in vitro* experiments only [23].

We also probed the cellular uptake of the Dox-conjugated nanoparticles using fluorescence microscopy of cells, after treatment of 2 hours. The intrinsic fluorescence of Dox was optically tracked. Figure 6B represents the fluorescence images of the treated cells, showing

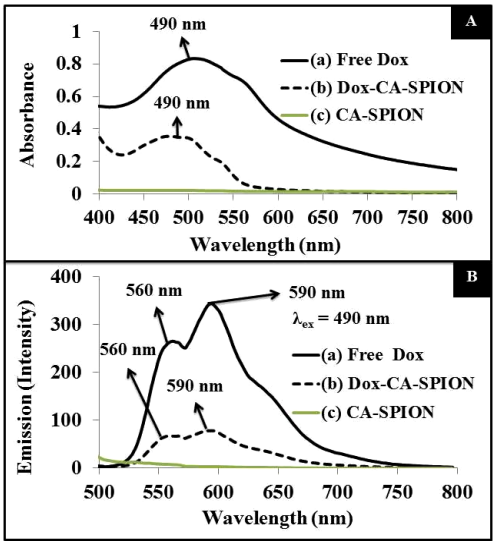

Figure 4: (A) Absorption, and (B) fluorescence spectra of free doxorubicin (Dox), CA-SPION, and Dox-conjugated CA-SPION (Dox-CA-SPION).

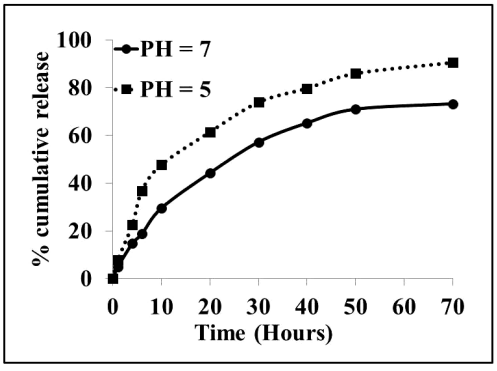

Figure 5: The time-dependent release study of Dox from Dox-CA-SPION at 37°C.

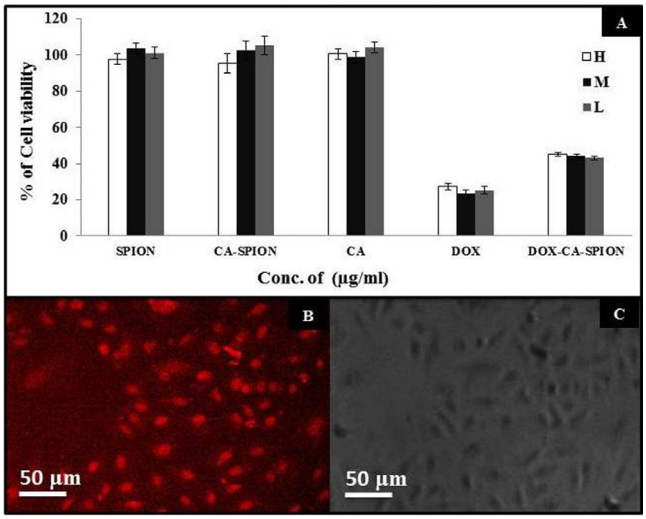

Figure 6: (A) Cell viability (MTT) assay probing possible cytotoxic effects of free doxorubicin (Dox, H=30 µg/mL, M=20 µg/mL, L=10 µg/mL), iron-oxide nanoparticles (SPION, H=400 µg/mL, M=200 µg/mL, L=100 µg/mL), iron-oxide nanoparticles coated citric acid (CA-SPION, H=500 µg/mL, M=250 µg/mL, L=125 µg/mL), free citric acid (CA, H=800 µg/mL, M=400 µg/mL, L=200 µg/mL) and doxorubicin conjugated iron-oxide nanoparticles (Dox-CA-SPION, H=400 µg/mL, M=200 µg/mL, L=100 µg/mL). Average values of three measurements are depicted, (B) Fluorescence microscopy analysis of cells treated with Dox-CA-SPION, showing fluorescent staining of treated cells and (C) Phase-contrast image of the same treated cells, showing their morphology.

robust optical signal (from Dox) from the cells (pseudo-colored in grayscale). Figure 6C shows the same cells in phase contrast. The treated cells looked morphologically healthy, further indicating the non-toxicity of particles. This experiment shows that the nanoparticles are efficient uptake by the cells, thus highlighting the promise of these nanoparticles also as non-toxic optical labels in bioimaging studies. The above experiments showed that the bioconjugated iron-oxide nanoparticles are passively taken up by cells *in vitro*, with no sign of non-specific toxicity.

Conclusion

In this study, we have shown the facile synthesis of drug conjugated superparamagnetic iron oxide nanoparticles in which citric acid could be readily coated to the surface of dox-SPIONs to release the drug in a sustained manner. *In vitro* studies probed that these nanoparticles have been efficiently up taken by the cells and cell uptake has been further enhanced upon magnetic guidance. CA-SPION nanoparticles were found to be non-toxic while their drug conjugates due to drug induced cytotoxicity were showing less cytotoxicity because of the slow release of the drug. The major therapeutic advantage of drug conjugated nanoparticles in magnetically targeted drug delivery is expected to be more pronounced in in vivo studies where the efficacy of free drug is negligible. Thus, future studies will be focused on optimizing the delivery of CA-SPIONs NPs in vivo using tumor-model animals.

Acknowledgement

We are grateful to the University of Delhi, India, for providing Research and Development grant to support this study. We thank Ms. Anuradha and Ms. Komal Sethi for their help related to cell culture work.

References

1. Davis SS (1997) Biomedical applications of nanotechnology--implications for drug targeting and gene therapy. Trends Biotechnol 15: 217-224.
2. Li K, Shen M, Zheng L, Zhao J, Quan Q, et al. (2014) Magnetic resonance imaging of glioma with novel APTS-coated superparamagnetic iron oxide nanoparticles. Nanoscale Res Lett 9: 304.
3. Sahoo B, Devi KS, Dutta S, Maiti TK, Pramanik P, et al. (2014) Biocompatible mesoporous silica-coated superparamagnetic manganese ferrite nanoparticles for targeted drug delivery and MR imaging applications. J Colloid Interface Sci 431: 31-41.
4. Yu X, Pishko MV (2011) Nanoparticle-based biocompatible and targeted drug delivery: characterization and *in vitro* studies. Biomacromolecules 12: 3205-3212.
5. Prasad PN (2004) Nanophotonics, Wiley–Interscience, New York.
6. Leuschner C, Kumar CS, Hansel W, Soboyejo W, Zhou J, et al. (2006) LHRH-conjugated magnetic iron oxide nanoparticles for detection of breast cancer metastases. Breast Cancer Res Treat 99: 163-176.
7. McGill SL, Cuylear CL, Adolphi NL, Osinski M, Member S, et al. (2009) Magnetically Responsive Nanoparticles for Drug Delivery Applications Using Low Magnetic Field Strengths. IEEE Transactions on Nanobioscience 8: 33-42.
8. Banerjee SS, Chen DH (2008) Multifunctional pH-sensitive magnetic nanoparticles for simultaneous imaging, sensing and targeted intracellular anticancer drug delivery. Nanotechnology 19: 505104.
9. Vasir JK, Labhasetwar V (2005) Targeted drug delivery in cancer therapy. Technol Cancer Res Treat 4: 363-374.
10. McCarthy JR, Weissleder R (2008) Multifunctional magnetic nanoparticles for targeted imaging and therapy. Adv Drug Deliv Rev 60: 1241-1251.
11. Gupta AK, Gupta M (2005) Synthesis and surface engineering of iron oxide nanoparticles for biomedical applications. Biomaterials 26: 3995-4021.
12. Sun C, Lee JS, Zhang M (2008) Magnetic nanoparticles in MR imaging and drug delivery. Adv Drug Deliv Rev 60: 1252-1265.
13. Duguet E, Vasseur S, Mornet S, Devoisselle JM (2006) Magnetic nanoparticles and their applications in medicine. Nanomedicine (Lond) 1: 157-168.
14. Ho D, Sun X, Sun S (2011) Monodisperse magnetic nanoparticles for theranostic applications. Acc Chem Res 44: 875-882.
15. Mojica Pisciotti ML, Lima E Jr, Vasquez Mansilla M, Tognoli VE, Troiani HE, et al. (2014) *In vitro* and *in vivo* experiments with iron oxide nanoparticles functionalized with DEXTRAN or polyethylene glycol for medical applications: magnetic targeting. J Biomed Mater Res B Appl Biomater 102: 860-868.
16. Tome P, Fierrez J, Vera-Rodriguez R, Ramos D (2013) Identification using face regions: application and assessment in forensic scenarios. Forensic Sci Int 233: 75-83.
17. Levy L, Sahoo Y, Kim KS, Bergey E, Prasad PN (2002) Nanochemistry: Synthesis and Characterization of Multifunctional Nanoclinics for Biological Applications. Chem Mater 14: 3715-3721.
18. Islam MS, Kurawaki J, Kusumoto Y, Abdulla-Al-Mamun M, Mukhlish MZB (2012) Hydrothermal Novel Synthesis of Neck-structured Hyperthermia-suitable Magnetic (Fe_3O_4, γ-Fe_2O_3 and α-Fe_2O_3) Nanoparticles. J Sci Res 4: 97-107.
19. Tassa C, Shaw SY, Weissleder R (2011) Dextran-coated iron oxide nanoparticles: a versatile platform for targeted molecular imaging, molecular diagnostics, and therapy. Acc Chem Res 44: 842-852.
20. Lee H, Lee E, Kim DK, Jang NK, Jeong YY, et al. (2006) Antibiofouling polymer-coated superparamagnetic iron oxide nanoparticles as potential magnetic resonance contrast agents for *in vivo* cancer imaging. J Am Chem Soc 128: 7383-7389.
21. Borthakur A, Mellon E, Niyogi S, Witschey W, Kneeland JB, et al. (2006) Sodium and T1rho MRI for molecular and diagnostic imaging of articular cartilage. NMR Biomed 19: 781-821.
22. Berry CC, Curtis ASG (2003) Functionalisation of magnetic nanoparticles for applications in biomedicine. J Phys D: Appl Phys 36: 198-206.
23. Santra S, Kaittanis C, Grimm J, Perez JM (2009) Drug/dye-loaded, multifunctional iron oxide nanoparticles for combined targeted cancer therapy and dual optical/magnetic resonance imaging. Small 5: 1862-1868.
24. Sahoo B, Sanjana K, Devi PS, Nayak SK, Maiti TK, et al. (2013) Facile preparation of multifunctional hollow silica nanoparticles and their cancer specific targeting effect. Biomater Sci 1: 647-657.

25. Nigam S, Barick KC, Bahadur D (2011) Development of citrate-stabilized Fe3O4 nanoparticles: Conjugation and release of doxorubicin for therapeutic applications. J Magn Magn Mater 323: 237–243.

26. Asrar SM, Sultan MAK, Altaff K (2012) Detergent Induced Histopathological Alterations to *Ctenopharyngodon idella*. Advanced BioTech 11: 24-26.

27. Ramesh R, Rajalakshmi M, Ramya SG, Muthamizhchelvan C, Suruttaiya UP, et al. (2011) Controllable Synthesis of Single-Crystalline Fe_3O_4 Nanorice by a One-Pot, Surfactant-Assisted Hydrothermal Method and Its Properties. Eur J Inorg Chem 35: 5384-5389.

28. Kumar P, Anuradha, Roy I (2014) Optically and magnetically doped ormosil nanoparticles for bio imaging: synthesis, characterization, and *in vitro* studies. RSC Advances 4: 16181-16187.

29. Sahoo Y, Goodarzi A, Swihart MT, Ohulchanskyy TY, Kaur N, et al. (2005) Aqueous ferrofluid of magnetite nanoparticles: Fluorescence labeling and magnetophoretic control. J Phys Chem B 109: 3879-3885.